Eur. Phys. J. Plus (2023) 138:170
https://doi.org/10.1140/epjp/s13360-023-03795-8

THE EUROPEAN PHYSICAL JOURNAL PLUS

Regular Article

The nonlinear optical properties of "12-6" tuned GaAs/GaAlAs double quantum well under the external fields

A. Turker Tuzemen[1,a], **H. Dakhlaoui**[2,3,b], **E. B. Al**[4,c], **F. Ungan**[4,d]

[1] Department of Mathematics and Science Education, Faculty of Education, Sivas Cumhuriyet University, 58140 Sivas, Turkey
[2] Basic and Applied Scientific Research Center (BASRC), College of Science of Dammam, Imam Abdulrahman Bin Faisal University, P. O. Box 1982, Dammam 31441, Saudi Arabia
[3] Department of Physics, College of Sciences for Girls, Imam Abdulrahman Bin Faisal University, Dammam, Saudi Arabia
[4] Department of Physics, Faculty of Science, Sivas Cumhuriyet University, 58140 Sivas, Turkey

Received: 12 December 2022 / Accepted: 11 February 2023

Abstract We have studied the linear and nonlinear optical properties of 12-6 GaAs/$Ga_{1-x}Al_xAs$ double quantum well heterostructure under different external fields' effects such as electric, magnetic and intense laser fields. We also investigated the effects of the variations of well width and aluminum concentration on the optical response of the structure under zero external field. Within the framework of effective mass and parabolic band approach, the time-independent Schrödinger equation has been solved numerically to obtain energy levels and the corresponding wave functions of the heterostructure by using the diagonalization method. The linear and nonlinear optical properties' expressions have been calculated with the help of the compact density matrix method. According to our numerical results, we obtain a blue (red) shift of the resonant peaks belonging to the total optical absorption coefficients and the refractive index change with increasing applied external fields (the width of the well and aluminum concentration).

1 Introduction

Today, many studies on low-dimensional heterostructures such as quantum wells (QWs), quantum well wires (QWWs) and quantum dots (QDs) are carried out. The electronic and optical properties of these heterostructures have significant roles in designing advanced optoelectronic device as laser diodes [1], light-emitting diodes [2], photodetectors [3], photodiodes [4], etc. QWs are the most intensively studied among these heterostructures because they have computational advantages mathematically and can be easily fabricated. The electronic and optical properties of the QWs are determinable by chosen suitable structure parameters such as the well's width and depth or applied external fields such as electric field, magnetic field and intense laser field (ILF) [5–16]. All these applied external fields change the profile of the confinement potential and hence the subband energies and the envelope wave functions of the structure. Besides these changes, the studies on this subject have shown that the linear and nonlinear optical coefficients of the heterostructure such as the optical absorption coefficients (OACs) and the refractive index changes (RICs) are affected sensitively by these external fields. For example, Karimi and Vafaei [17] have studied the effects of ILF on the OACs and RICs for a strained InGaN/GaN QW structure. They showed that the resonant peaks shifted to red in the case of increasing ILF. In their work, Ungan et al. [18] investigated how the ILF and electric field affected the total OAC (TOAC) and RIC (TRIC) in GaInNAs/GaAs double QWs and they determined that when applied electric field have been increased, TOAC and TRIC shifted toward higher energies with decreasing. Moreover, it was found that the peak positions of increasing TOAC and TRIC as the ILF increased have not changed nearly. The OACs and RICs of $Al_xGa_{1-x}As$/GaAs staircase-like QWs structure under the effects of electric, magnetic and ILF have been examined by Dakhlaoui et al. [19]. They obtained that the OACs and the RICs could be blueshifted and redshifted by increasing the electric field and the ILF, respectively. At the same time, they found out interestingly that it could be obtained either a blueshift or redshift by setting the applied magnetic field. In another study, Turkoglu et al. [20] examined the effects of applied external fields such as ILF, electric and magnetic fields on the optical properties of a GaAs QW structure that had Razavy confinement potential, and they have obtained that the peak positions of OACs and RICs showed more clear changes in the case of increasing the intense laser and electric fields according to the case of increasing magnetic field.

[a] e-mail: atuzemen@cumhuriyet.edu.tr
[b] e-mail: h_dakhlaoui@yahoo.fr
[c] e-mail: emrebahadiral@hotmail.com
[d] e-mail: fungan@cumhuriyet.edu.tr (corresponding author)

Published online: 22 February 2023

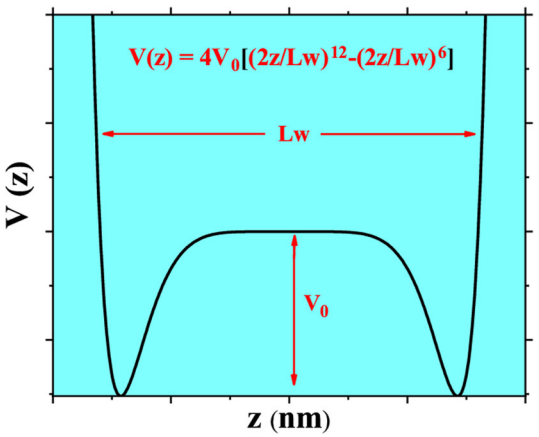

Fig. 1 Schematic diagram of 12-6 double QW which is investigated in the study. The width and the barrier height of the structure are Lw and $V_{0,}$ respectively, and during investigating the effects of external fields they are taken as constant values Lw = 16nm and V_0 = 228meV

The focus of the present work is examining the changes in the linear and nonlinear optical properties of 12-6 GaAs/$Ga_{1-x}Al_xAs$ double QW heterostructure in the case of applying different external fields such as ILF, electric and magnetic fields separately. Moreover, the effects of structural parameters such as QW's width (Lw) and aluminum concentration (x) on the changes in these optical properties will be investigated. To achieve our goals, firstly we will solve numerically the Schrödinger equation by using the diagonalization method to obtain the subband energy levels and the corresponding wave functions of the structure within the effective mass and parabolic band approximation. And then we will obtain the analytical expressions of the linear and nonlinear optical properties by using the compact density matrix method. Our article's organization is as follows: The formulation and theoretical calculations of the problem and achieved numerical results with discussions are presented in the second and third sections, respectively. In the last section, our conclusions are given.

2 Theory

In this study, the investigated heterostructure is "12-6" GaAs/$Ga_{1-x}Al_xAs$ double QW, which have two symmetric wells coupled with a barrier as shown in Fig. 1. While the direction of the electric field ($\mathbf{F} = F\widehat{z}$) is chosen as parallel to the growth direction of the QW structure, the magnetic field ($\mathbf{B} = B\widehat{x}$) is taken as perpendicular to the growth direction. In addition, the ILF is oriented along the z-axis.

The total Hamiltonian for an electron confining in the heterostructure as shown in Fig. 1 with the effects of the external fields mentioned above and the use of effective mass and parabolic band approaches can be given as [21]

$$\mathcal{H} = \frac{1}{2m^*}\left[\boldsymbol{p} + \frac{e}{c}\boldsymbol{A}(\boldsymbol{r})\right]^2 + V(z,\alpha_0) + eFz \tag{1}$$

The effective mass and the charge of the electron are m^* and e, respectively. $\boldsymbol{p}$ expresses the momentum operator, c is the light's velocity, and $\boldsymbol{A}(\boldsymbol{r})$ $(= -Bz\widehat{y})$ is the vector potential of the magnetic field. F is the electric field's strength, and $V(z,\alpha_0)$ is the laser dressed confinement potential. The value of $V(z,\alpha_0)$ is obtained through integrating numerically the expression given below [22, 23]

$$V(z,\alpha_0) = \frac{\varpi}{2\pi}\int_0^{\frac{2\pi}{\varpi}} V(z+\alpha_0 \sin\varpi t)dt, \tag{2}$$

where ϖ shows the nonresonant frequency of the laser field, $\alpha_{0,}$ which equals to $\frac{eF_0}{m^*\varpi}$ is the laser dressing parameter. F_0 expresses the strength of the laser field. $V(z)$ is the confinement potential of the structure in the case of no ILF and written as:

$$V(z) = 4\mathrm{V}_0\left[\left(\frac{2z}{\mathrm{Lw}}\right)^{12} - \left(\frac{2z}{\mathrm{Lw}}\right)^{6}\right], \tag{3}$$

where the structure parameters V_0 and Lw are the barrier height and well width, respectively. The expression of the potential barrier height, which depends on mole fraction (x) of Al in $Ga_{1-x}Al_xAs$, is given by [24]

$$V_0(x) = 0,6 \times \Delta E_g^{\Gamma}(x), \tag{4}$$

where $\Delta E_g^{\Gamma}(x)$ expresses the changing the band gap energies' difference of the GaAs and $Ga_{1-x}Al_xAs$ at point Γ and it equals $\Delta E_g^{\Gamma}(x) = \left(1,115x + 0,37x^2\right)eV$.

In order to reveal the effects of the applied external fields on the linear and nonlinear optical properties of the structure, we have obtained the solution of the eigensystem ($\mathcal{H}\varphi_i(z) = E_i\varphi_i(z)$) by using diagonalization method [25].

$$-\frac{\hbar^2}{2m^*}\frac{d^2\varphi_i(z)}{dz^2} + \left[\frac{e^2B^2}{2m^*c^2}z^2 + V(z,\alpha_0) + eFz\right]\varphi_i(z) = E_i\varphi_i(z), \tag{5}$$

where E_i and $\varphi_i(z)$ stand the energy eigenvalues and the corresponding wave functions for each level. The diagonalization method is based on explaining the wave functions of the electron-$\varphi_i(z)$ in terms of complete set of orthonormal functions of potential well with infinite barriers as expressed in [26–28]

$$\varphi_i(z) = \sqrt{\frac{2}{L_\infty}}\sum_n C_n \sin\left(\frac{n\pi z}{L_\infty} + \frac{n\pi}{2}\right) \tag{6}$$

The well's width L_∞ is selected as remarkably larger than the width of the studied structure, C_n is the expansion coefficient, and n is a positive integer. Following the calculations of the energy eigenvalues and the corresponding wave functions, we acquired the equations of the TOAC and the TRIC belonging the mentioned QW system. These values depend on the transition energy difference ($\Delta E = E_2 - E_1$) between the ground and the first excited states and the electric dipole moment matrix element given as $M_{ij} = \langle\varphi_i(z)|ez|\varphi_j(z)\rangle$, $(i, j = 1, 2)$. The OACs have been obtained from the compact density matrix method with iterative procedure [29–31]:

$$\beta^1(\omega) = \omega\sqrt{\frac{\mu_0}{\varepsilon_r}}\frac{|M_{21}|^2\sigma_v(\hbar/\tau_{12})}{(\Delta E - \hbar\omega)^2 + (\hbar/\tau_{12})^2} \tag{7}$$

$$\beta^3(\omega, I) = -2\omega\sqrt{\frac{\mu_0}{\varepsilon_r}}\left(\frac{I}{\varepsilon_0 n_r c}\right)\frac{|M_{21}|^4\sigma_v(\hbar/\tau_{12})}{\left[(\Delta E - \hbar\omega)^2 + (\hbar/\tau_{12})^2\right]^2} \times\left[1 - \frac{|M_{22} - M_{11}|^2}{|2M_{21}|^2}\times\frac{\left(3(\Delta E)^2 - 4\Delta E\hbar\omega + \hbar^2\left(\omega^2 - \left(1/\tau_{12}^2\right)\right)\right)}{(\Delta E)^2 + (\hbar/\tau_{12})^2}\right] \tag{8}$$

The TOAC is written as the sum of Eqs. (7) and (8):

$$\beta(\omega, I) = \beta^1(\omega) + \beta^3(\omega, I). \tag{9}$$

In obtained expressions, while ω shows the incident photon's angular frequency, $\hbar$ and τ_{12} are the value of reduced Planck constant and inter-subband relaxation time, respectively. The other constants are as follows: μ_0 is the magnetic permeability, ε_r is the dielectric permittivity, σ_v is the carrier density in the inter-subband transition, ε_0 is the permittivity value of free space, n_r is the refractive index, and I is the electromagnetic field's intensity.

With the same procedure, the RICs have been obtained as

$$\frac{\Delta n^1(\omega)}{n_r} = \frac{\sigma_v|M_{21}|^2}{2n_r^2\varepsilon_0}\frac{\Delta E - \hbar\omega}{(\Delta E - \hbar\omega)^2 + (\hbar/\tau_{12})^2} \tag{10}$$

and

$$\frac{\Delta n^3(\omega, I)}{n_r} = -\frac{\mu_0 c}{4n_r^3\varepsilon_0}\frac{|M_{21}|^2\sigma_v I}{\left[(\Delta E - \hbar\omega)^2 + (\hbar/\tau_{12})^2\right]^2}\left[4(\Delta E - \hbar\omega)|M_{21}|^2 - \frac{(M_{22} - M_{11})^2}{(\Delta E)^2 + (\hbar/\tau_{12})^2} \times\left[(\Delta E - \hbar\omega)\left(\Delta E(\Delta E - \hbar\omega) - (\hbar/\tau_{12})^2\right) - (\hbar/\tau_{12})^2(2\Delta E - \hbar\omega)\right]\right] \tag{11}$$

The TRIC is found as,

$$\frac{\Delta n(\omega, I)}{n_r} = \frac{\Delta n^1(\omega)}{n_r} + \frac{\Delta n^3(\omega, I)}{n_r}. \tag{12}$$

The physical parameters and constants we use in our work are [28]: The width of the structure and the barrier height are Lw = 16nm and $V_0 = 228meV$ (for $x = 0.3$), respectively (during investigation the effects of external fields). $m^* = 0.067m_0$ (where m_0 is the free electron mass), $\varepsilon_r = 12.58$, $\varepsilon_0 = 8.854 \times 10^{-12}$, $e = 1.602 \times 10^{-19}C$, $\hbar = 1.056 \times 10^{-34}Js$, $\sigma_v = 3 \times 10^{22}\mathrm{m}^{-3}$, $n_r = 3.2$, $\mu_0 = 4\pi \times 10^{-7}\mathrm{Hm}^{-1}$, $\tau_{12} = 0.14ps$ and $I = 0.1 \times 10^{10}\mathrm{MW/cm}^2$.

3 Results and discussion

Firstly, we investigated the effects of the electric, magnetic and ILF on the structure of confining potential and the probability densities for the lowest two energy levels by taking as Lw = 16nm and$V_0 = 228meV$. In Fig. 2(a), we can mention that the probability densities are almost symmetric according to the QW's midpoint in the absence of the external fields (F = 0, B = 0

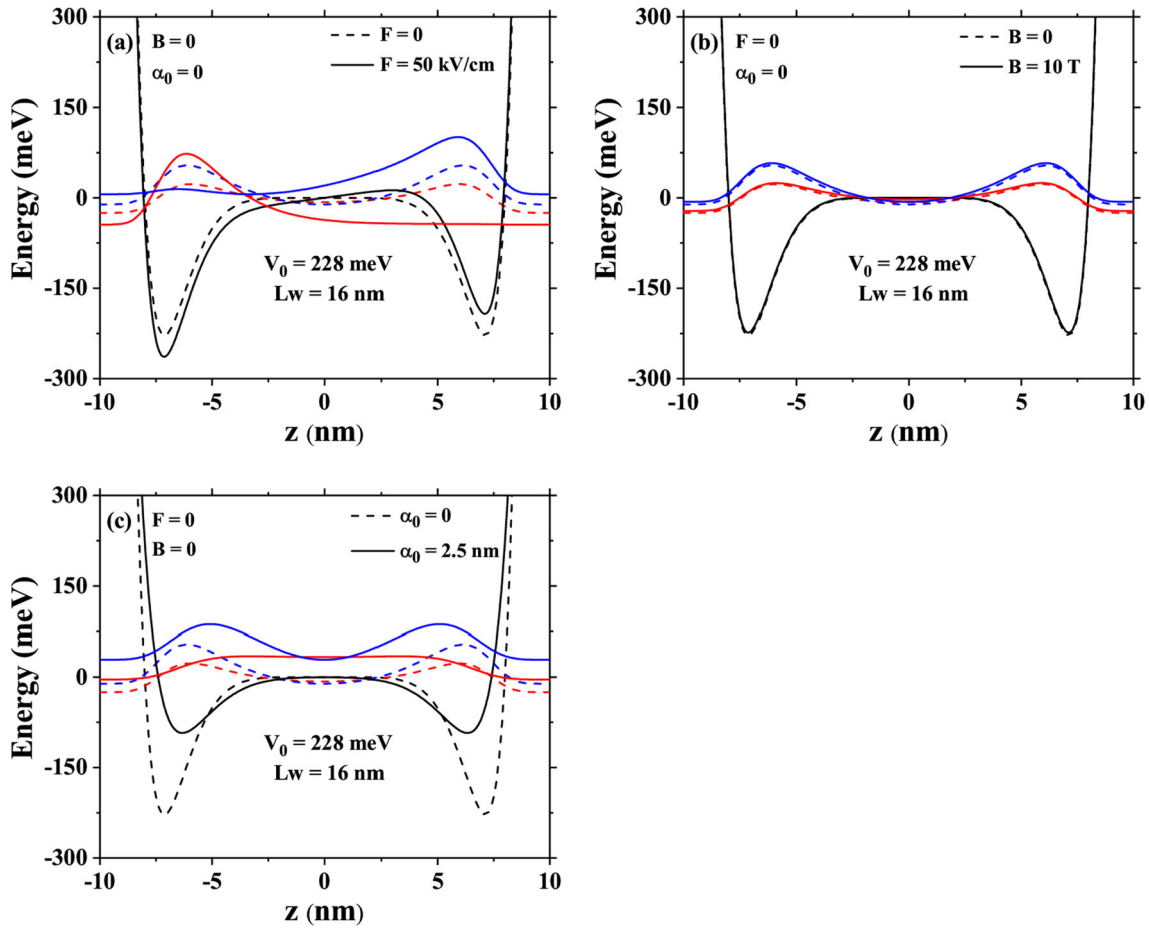

Fig. 2 The changes of 12-6 double QW confinement potential and the probability density for the envelope wave functions of the ground and first excited states under the effect of the (**a**) electric field, **b** magnetic field and (**c**) intense laser field

and$\alpha_0 = 0$). In this case, both the ground level and the first excited level have a peak in each well. Therefore, when the particle is in the ground or the first excited state, it can be found on either the right or the left well with equal possibility. Also Fig. 2(a) shows the effect of the electric field which is applied along the growth direction, when the magnetic and intense laser fields are zero (B $= 0$ and$\alpha_0 = 0$). With the applied electric field, a deeper region is formed in the left side of the structure. In this case, since the charge carriers will move toward the deeper potential region, the symmetries in the probability densities are damaged. Since the electron is pushed to the left-hand side of the structure by the electric field while the localization of the electron decreases in the right well, it increases in the left well for the ground state. In contrast to the ground state, electron's localization increases in the right well for the first excited state due to the orthogonality relation between $\varphi_1(z)$ and$\varphi_2(z)$. The shift of $\varphi_1(z)$ toward the left well is a consequence of Stark effect introduced by the electric field. Furthermore, we observe that the bottom of the left well is pushed downward. For this reason, the energy level of ground state is E_1 slightly diminished. On the other hand, the bottom of the right well rises under the electric field action leading to an increase in the energy level of the first excited state E_2. This opposite variation between E_1 and E_2 is important since it leads to enlarging the energy separation $(E_2 - E_1)$ by augmenting the electric field and a displaying a blueshift in the (TOAC).

We examine how the potential profile and the probability densities change by applying only magnetic field perpendicular to the direction of growth (F $= 0$ and $\alpha_0 = 0$) in Fig. 2(b). Both the symmetries of the potential profile and the probability densities are not affected by applied magnetic field as seen from the figure. Only a very slightly change in probability densities is occurred. Contrarily to the electric field which tilts the shape of the confining potential, the magnetic field introduces additional parabolic confinement per respect to the origin of the structure (z $= 0$). This means that the total potential maintains its symmetric shape, and per consequent, the wave function profiles and energy levels remain practically unchanged.

Figure 2(c) shows the effects of applied ILF on the confining potential and the probability densities in the case of F $= 0$ and B $= 0$. With the applied ILF, both the width (Lw) and the barrier height (V_0) of the structure decrease. At the same time, there is also a decrease in the depth of the wells because the well base values are moved to higher. The reason for this change is the increase in the energy gap value of the semiconductor where the laser field is applied. In this case, the levels of the subband energies have

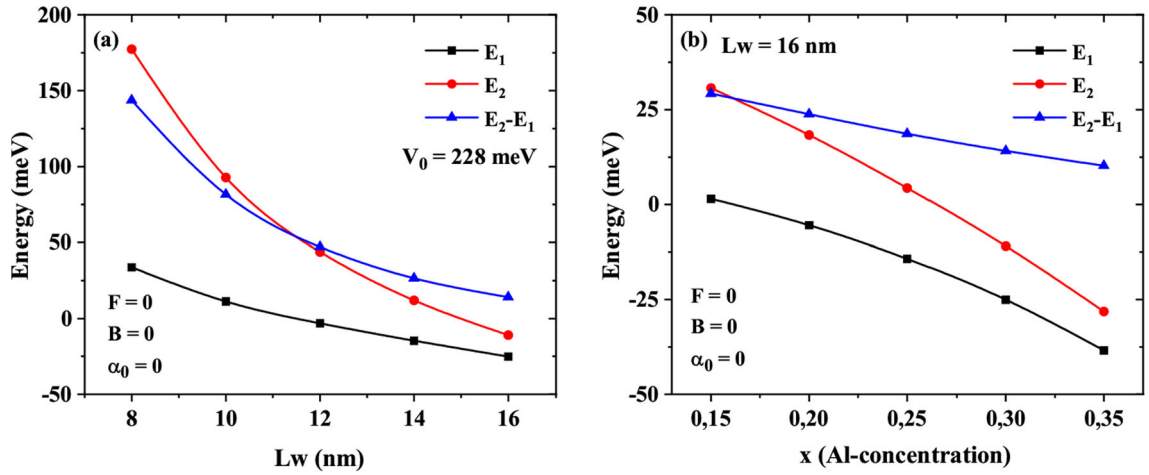

Fig. 3 Variations of the lowest two energy levels and the difference between them in the absence of the external fields (F = 0, B = 0 and $\alpha_0 = 0$) as a function of the (**a**) width of the heterostructure (Lw) for $V_0 = 228$meV, **b** aluminum concentration (x) for Lw = 16nm

higher values and an increase occurs the difference between them. In addition, the ILF maintains the symmetry of the potential with respect to (z = 0) which explains the symmetrical behavior of the density of probabilities.

The investigations of the lowest two energy levels and the differences between them in the case of no external fields are given in Fig. 3 while the changes in energies and their differences are examined as a function of the width of the structure (Lw) in Fig. 3(a). In Fig. 3(b), they are studied as a function of aluminum concentration (x). In the first case, we changed the values of Lw as 8nm, 10nm, 12nm, 14nm and 16nm for $V_0 = 228$meV. Increasing in the value of Lw gives rise to a decrease in energy difference between the ground and first excited states because of the decrease in spatial localization. The value of aluminum concentration (x) has been changed from 0, 15 to 0, 35 in 0, 05 increments for constant Lw value in Fig. 3(b). At higher Al concentration values, the deeper potential wells are obtained. Similar to Fig. 3(a), there is a decrease in the energy difference with increasing Al concentration. With these, decreases in the energy differences cause to the redshift of the TOACs' and TRICs' resonant peaks. Moreover, when two figures are compared, it can be seen that decreasing in difference between electron subband energies with increasing well width is faster compared to the case with increasing Al concentration. In other words, the energy levels are more sensitive to the quantum size (depth of wells) than to the aluminum concentration.

In Fig. 4, we plot again the changes in lowest two energy levels and the differences between them. But this time, we obtain the energy changes and differences according to increasing of electric field (F), magnetic field (B) or the laser dressing parameter ($_0$). We take the values of the well's width and the barrier's height as Lw = 16nm and $V_0 = 228$meV, respectively. In all three cases, the variations of the energy differences have the same behavior, and they increase with the increase in the strength of F, B or $_0$. This increase in the energy difference leads to the blueshift of the resonant peaks of the TOAC and TRIC. In addition, while the lowest change in energy differences was obtained with magnetic field change, the highest change was obtained with laser field change. The reason for this result is the effects, which can be seen from Fig. 2 on the confining potential profile of the applied external fields.

In Fig. 5, changes in the occupation ratio factor (f_{12}) and dipole moment matrix elements (M_{12}) are plotted as functions of the heterostructure width and aluminum concentration under the same conditions used in Fig. 3. If the figures are examined, it can be seen that as both well width and Al concentration increase, the values of the occupation ratio factor decrease while the values of the dipole moment matrix elements increase. Here, while the behavior of the f_{12} determines the variation of the peak amplitudes of TOACs', M_{12}'s behavior plays a role in changes of the amplitudes of TRICs'.

The variations of the occupation ratio factor (f_{12}) and dipole moment matrix elements (M_{12}) as a function of the electric field, the magnetic field and the laser dressing parameter are reported separately in Fig. 6. In this investigation, the values of V_0 and Lw are taken as 228meV and 16nm, respectively. As seen from Figs. 6(a-c), with increasing the strength of the electric field, the magnetic field and the laser dressing parameter, M_{12} value decreases. The decrease behavior of M_{12} is different according to the applied external field, and this behavior defines changes of the amplitudes of TRICs'. While the value of f_{12} increases similarly for magnetic and intense laser fields, it decreases for electric field. These changes show us that TOACs' peak amplitudes increase (decrease) with the magnetic field's and the laser dressing parameter's increase (electric field's increase).

In Fig. 7, TOAC is plotted versus incident photon energy for different values of the width of the heterostructure (Lw) and Al concentration (x) under zero external field condition. In Fig. 7(a), while the value of V_0 is kept constant as $228meV$, L_w values are taken as 8 nm, 10nm, 12nm, 14nm and 16nm. Moreover, in the second figure, when the value of L_w is 16nm, the values of Al concentration (x) alter from 0, 15 to 0, 35 in 0, 05 increments. During this investigation, we obtained that as long as both the structure's width and Al concentration increase; the TOACs' amplitude and resonant peak position decrease and shift to lower energies

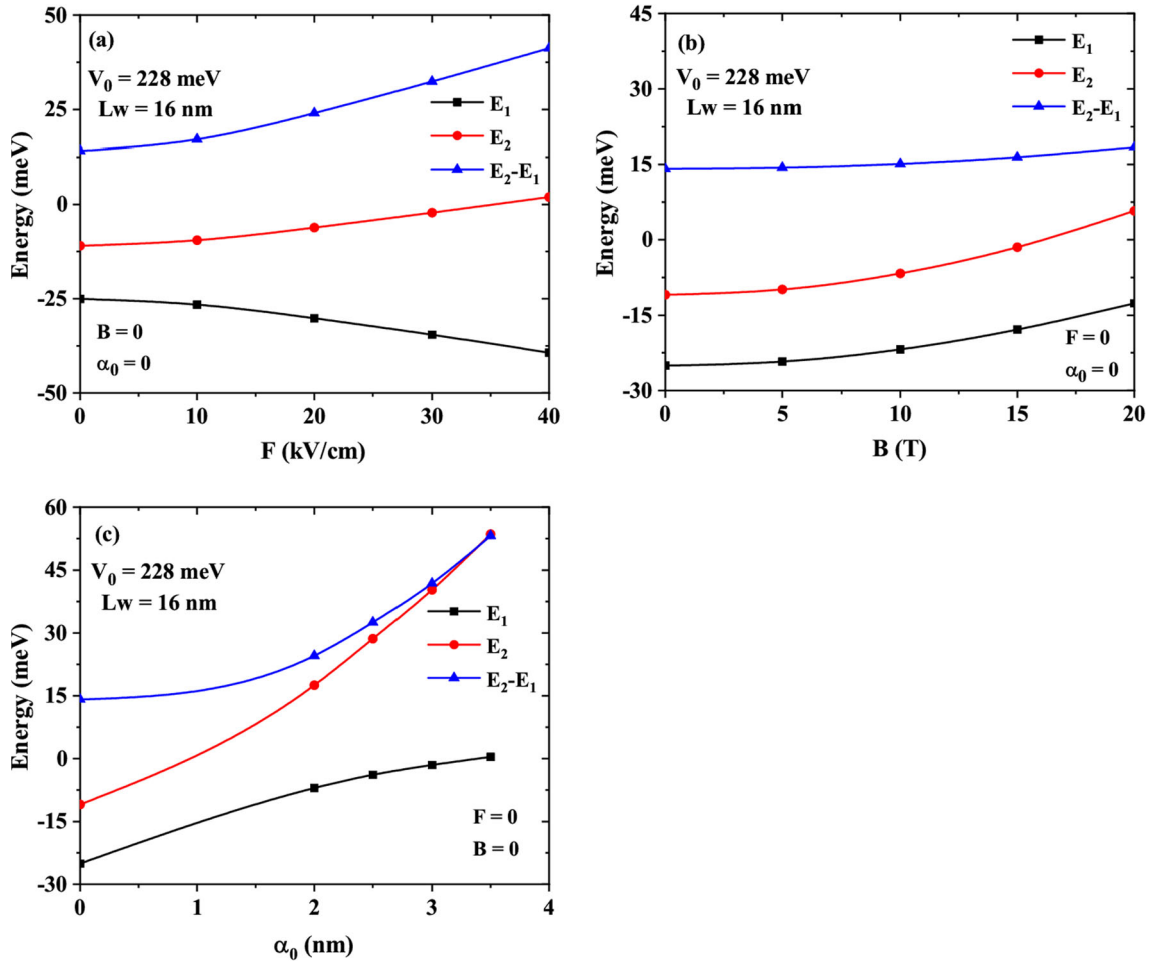

Fig. 4 Changes in the ground and first excited states and the energy difference between them for $V_0 = 228$meV and Lw $= 16$nm as a function of (**a**) the electric field in the case of B $= 0$ and $\alpha_0 = 0$, **b** the magnetic field in the case of F $= 0$ and $\alpha_0 = 0$, **c** the laser dressing parameter in the case of F $= 0$ and $B = 0$

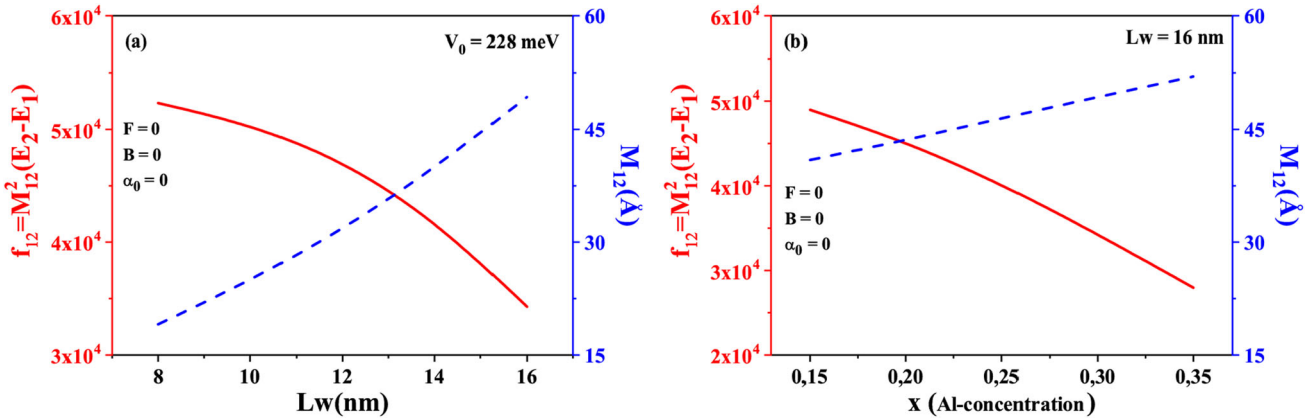

Fig. 5 Variations of the occupation ratio factor (f_{12}) and dipole moment matrix elements (M_{12}) when all external fields are zero as a function of the (**a**) width of the heterostructure (Lw) for $V_0 = 228$meV, **b** aluminum concentration (x) for Lw $= 16$nm

(redshift), respectively. This result is consistent with the variations of subband energy difference ($E_2 - E_1$) and the occupation ratio factor (f_{12}) obtained in Figs. 3 and 5, respectively.

We present in Fig. 8 the effects of different values of the electric field (F), magnetic field (B) and laser dressing parameter ($_0$) separately on TOACs' changes plotted versus incident photon energy. The other parameters used during this examination are $V_0 = 228$meV and Lw $= 16$nm. Looking at the figures, it is seen that the signal is shifted toward blue in all three cases as explained

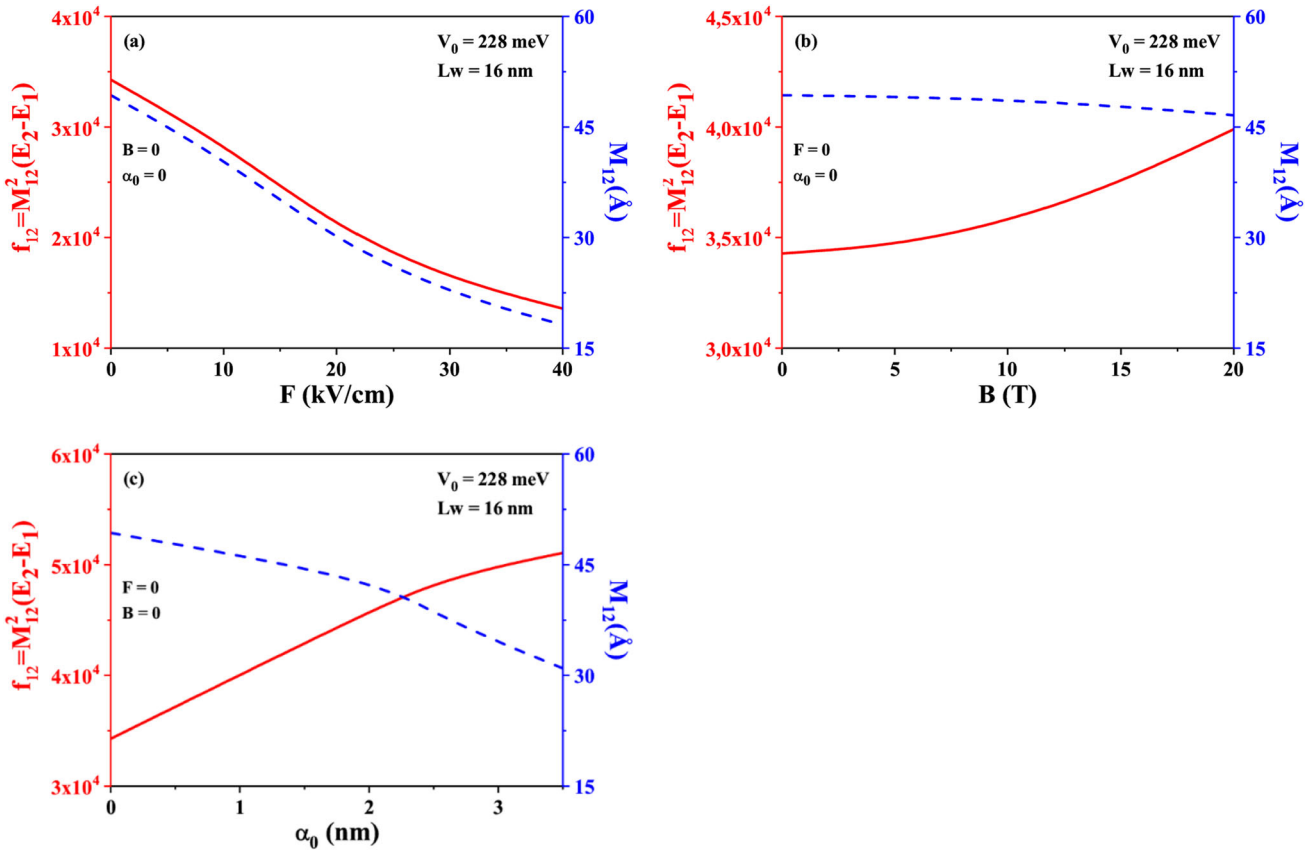

Fig. 6 Variations of the occupation ratio factor (f_{12}) and dipole moment matrix elements (M_{12}) for $V_0 = 228$meV and Lw $= 16$nm as a function of (**a**) the electric field in the case of B $= 0$ and $\alpha_0 = 0$, **b** the magnetic field in the case of F $= 0$ and $\alpha_0 = 0$, **c** the laser dressing parameter in the case of F $= 0$ and $B = 0$

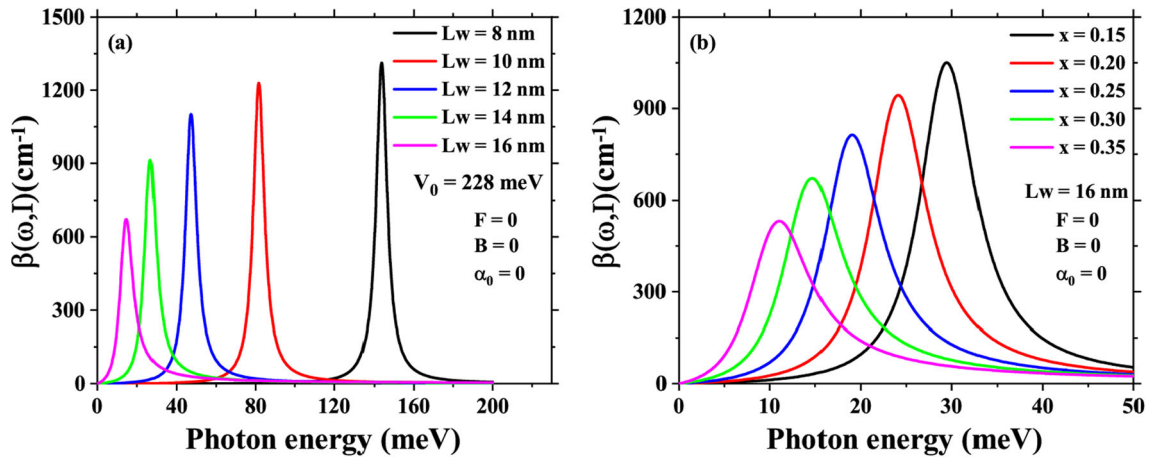

Fig. 7 In the absence of the external fields (F $= 0$, B $= 0$ and $\alpha_0 = 0$), the variations of TOAC for inter-subband transitions as a function of the incident photon energy for different values of the (**a**) width of the heterostructure (Lw) and (**b**) aluminum concentration (x)

in Fig. 4. The difference between them is that while the amplitude value of TOAC decreases with the increase in the electric field, the amplitude value increases in the case of the increase in the magnetic field and laser dressing parameter. The variations of f_{12} in Fig. 6 obtained under the conditions here support this result.

In the last part of our study, in Figs. 9 and 10 we examine the effects of the variations of the heterostructure width (L_w), Al concentration (x) and the external fields (F, B and α_0) on inter-subband TRICs, respectively. In Fig. 9, under zero external field we change the L_w values as 8 nm, 10nm, 12nm, 14nm and 16nm at constant V_0 (228meV) and the concentration of Al as 0, 15, 0, 20, 0, 25, 0, 30 and 0, 35 at constant structure width (16nm). For these cases, we observe that both when the values of the L_w

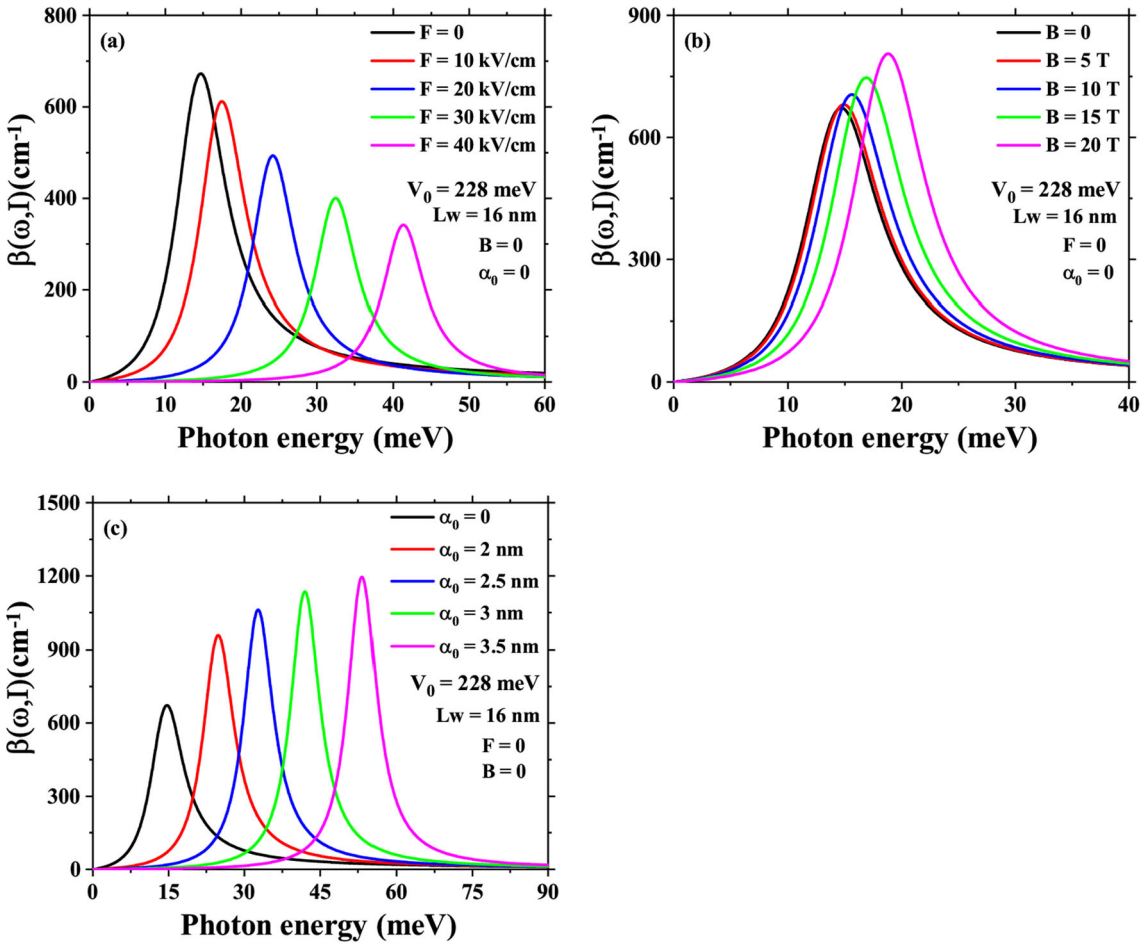

Fig. 8 The variations of TOACs for inter-subband transitions as a function of the incident photon energy for different values of the (**a**) electric field when B = 0 and $\alpha_0 = 0$, **b** magnetic field when F = 0 and $\alpha_0 = 0$, **c** laser dressing parameter when F = 0 and $B = 0$

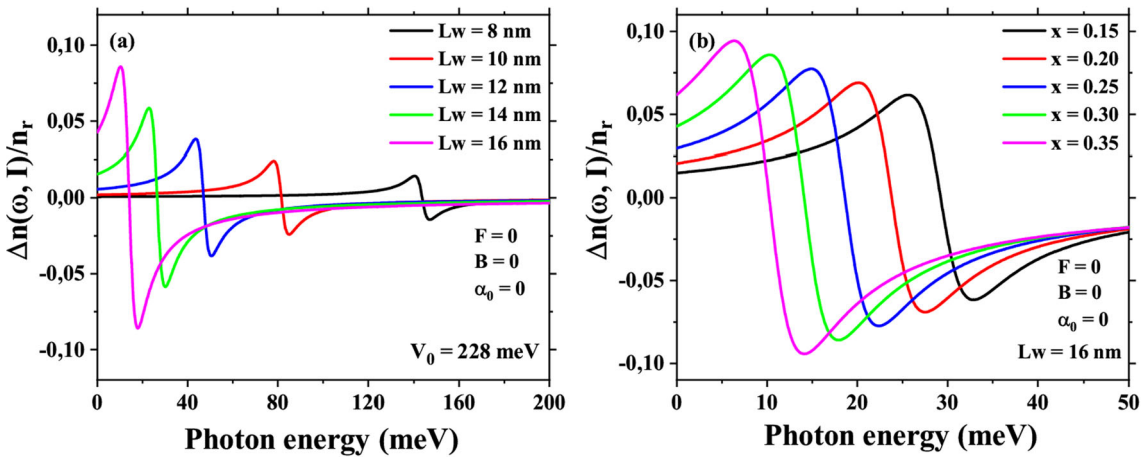

Fig. 9 For inter-subband transitions TRICs as a function of the incident photon energy for different values of the (**a**) width of the heterostructure (Lw) and (**b**) Al concentration (x)

and x augment, the amplitude of the TRICs increases and the signal undergoes a redshift. It can be seen from Fig. 5 that the value of the electric dipole matrix element increases with the increments in L_w, x and this increment clarifies the growth of amplitude. Additionally, as noticed from Fig. 3, decrease in inter-subband transition energy with increasing well width and Al concentration supports that TRICs have a redshift.

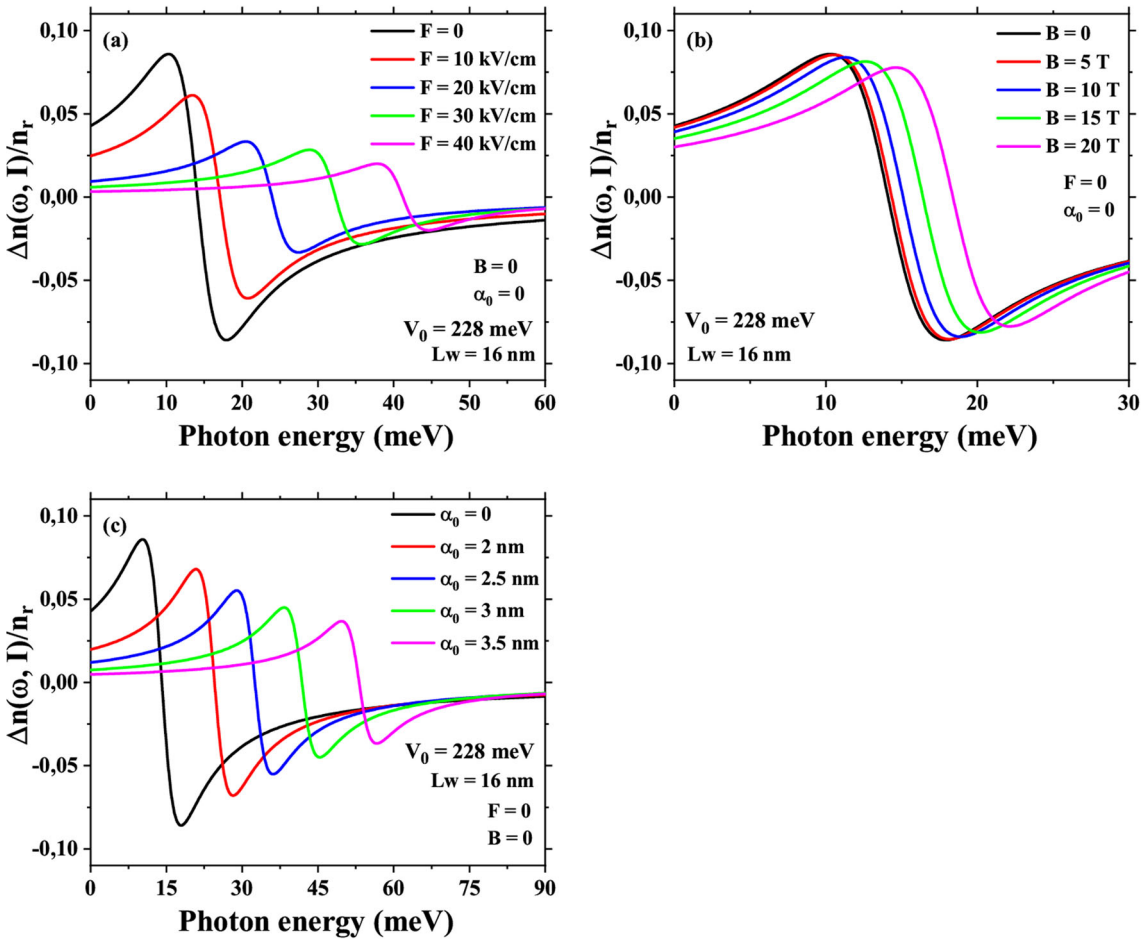

Fig. 10 For inter-subband transitions TRICs) as a function of the incident photon energy for different values of the (**a**) electric field in the case of B = 0 and $\alpha_0 = 0$, **b** magnetic field in the case of F = 0 and $\alpha_0 = 0$, **c** laser dressing parameter in the case of F = 0 and $B = 0$

In Fig. 10, TRICs are discussed for the structure which has the same conditions with Fig. 8. TRICs shift to higher energies and their amplitudes decrease during the increase in F, B and α_0 in all figures. While the changes in the energy difference between the ground and first excited states obtained in Fig. 4 support the shift to higher energies that occurs here, dipole matrix elements' variations in Fig. 6 explain the decrement in TRICs amplitude.

4 Conclusions

In our paper, we have done a theoretical study of the TOAC and TRIC relating to the inter-subband transition between the lowest two states for a 12-6 GaAs/$Ga_{1-x}Al_xAs$ double QW heterostructure under the effects of applied different external fields such as ILF, electric and magnetic fields separately. Besides the external fields' effects, we have investigated how these optical properties are affected from the variations of well width (Lw) and aluminum concentration (x) under zero external field. We solved numerically the Schrödinger equation by using diagonalization method to obtain the subband energy levels and the corresponding wave functions of the heterostructure within the effective mass approximation. As the next step, we acquired the analytical expressions of the linear and nonlinear optical properties by using compact density matrix method. The results from this study have showed that applied external fields, QW width and Al concentration affected the threshold energies of inter-subband transition, the TOAC and TRIC. According to obtained results, the resonant peak's position of the TOAC and the resonant peaks of the TRIC shift to higher energy regions (blueshift) when applied external fields increase. In the cases of increase in the width of QW and Al concentration, they shift to lower energies (redshift). Thus, it can be said that the resonant peak's position of the TOAC, the resonant peaks of the TRIC and their magnitudes can be adjusted by varying the strengths of the applied external fields, the values of the QW's width and Al concentration. The key point here is that the optical response can be effortlessly controlled through the chosen parameter, permitting us to modify the optoelectronic features within the THz range. This highlights the versatility of the "12-6" tuned GaAs/AlGaAs potential profile as a quantum well potential for potential THz devices. Note that the present work can be enlarged to study the

optical and electronic properties of spherical quantum dots based on "12-6" potential. Such studies are under investigation and will be published later.

Data Availability Statement This manuscript has associated data in a data repository. [Authors' comment: Data will be made available on request.]

References

1. Y. Alahmadi, P. LiKamWa, Effects of selective area intermixing on InAlGaAs multiple quantum well laser diode. Semicond. Sci. Technol. **34**, 025010 (2019). https://doi.org/10.1088/1361-6641/aaf439
2. S.-H. Lim, Y.-H. Ko, Y.-H. Cho, A quantitative method for determination of carrier escape efficiency in GaN-based lightemitting diodes: a comparison of open- and short-circuit photoluminescence. Appl. Phys. Lett. **104**, 091104 (2014). https://doi.org/10.1063/1.4867238
3. H.X. Wang, Z.L. Fu, D.X. Shao, Z.Z. Zhang, C. Wang, Z.Y. Tan, X.G. Guo, J.C. Cao, Broadband bias-tunable terahertz photodetector using asymmetric GaAs/AlGaAs step multi-quantum well. Appl. Phys. Lett. **113**, 171107 (2018). https://doi.org/10.1063/1.5046881
4. H. Lu, B. Zhang, F. Guo, The photocurrent-voltage characteristic simulated of resonant tunneling photodiodes. Opt. Quant. Electron **48**, 181 (2016). https://doi.org/10.1007/s11082-016-0373-9
5. E. Kasapoglu, F. Ungan, C.A. Duque, U. Yesilgul, M.E. Mora-Ramos, H. Sari, I. Sökmen, The effects of the electric and magnetic fields on the nonlinear optical properties in the step-like asymmetric quantum well. Phys. E **61**, 107 (2014). https://doi.org/10.1016/j.physe.2014.03.024
6. R.-Y. Yan, J. Tang, Z.-H. Zhang, J.-H. Yuan, Optical properties in GaAs/AlGaAs semiparabolic quantum wells by the finite difference method: combined effects of electric field and magnetic field. Int. J. Mod. Phys. B **32**, 1850159 (2018). https://doi.org/10.1142/S021797921850159X
7. H. Dakhlaoui, M. Nefzi, Tuning the linear and nonlinear optical properties in double and triple δ—doped GaAs semiconductor: Impact of electric and magnetic fields. Superlatt. Microstruct. **136**, 106292 (2019)
8. F. Ungan, M.K. Bahar, J.C. Martinez-Orozco, M.E. Mora-Ramos, Optical responses in asymmetric hyperbolic-type quantum wells under the effect of external electromagnetic fields. Photon. Nanostruct. Fundam. Appl. **41**, 100833 (2020)
9. E.C. Niculescu, L.M. Burileanu, A. Radu, Density of impurity states of shallow donors in a quantum well under intense laser field. Superlatt. Microstruct. **44**, 173 (2008). https://doi.org/10.1016/j.spmi.2008.03.005
10. F.M.S. Lima, M.A. Amato, O.A.C. Nunes, A.L.A. Fonseca, B.G. Enders, E.F. Da Silva, Unexpected transition from single to double quantum well potential induced by intense laser fields in a semiconductor quantum well. J. Appl. Phys. **105**, 123111 (2009). https://doi.org/10.1063/1.3153963
11. A.J. Peter, The effect of laser field intensity on polarizability in a quantum well. Phys. Lett. A **374**, 2170 (2010). https://doi.org/10.1016/j.physleta.2010.03.025
12. E. Ozturk, Nonlinear optical absorption in graded quantum wells modulated by electric field and intense laser field. Eur. Phys. J. B **75**, 197 (2010). https://doi.org/10.1140/epjb/e2010-00133-3
13. C.A. Duque, M.E. Mora-Ramos, E. Kasapoglu, H. Sari, I. Sökmen, Combined effects of intense laser field and applied electric field on exciton states in GaAs quantum wells: transition from the single to double quantum well. Phys. Status Solidi B **249**, 118 (2012). https://doi.org/10.1002/pssb.201147250
14. U. Yesilgul, E.B. Al, J.C. Martínez-Orozco, R.L. Restrepo, M.E. Mora-Ramos, C.A. Duque, F. Ungan, E. Kasapoglu, Linear and nonlinear optical properties in an asymmetric double quantum well under intense laser field: effects of applied electric and magnetic fields. Opt. Mater. **58**, 107e112 (2016). https://doi.org/10.1016/j.optmat.2016.03.043
15. I. Altuntas, H. Dakhlaoui, M.E. Mora-Ramos, F. Ungan, Combined effects of electric, magnetic, and intense terahertz laser fields on the nonlinear optical properties in GaAs/GaAlAs quantum well with exponentially confinement potential. Eur. Phys. J. Plus **136**, 1174 (2021). https://doi.org/10.1140/epjp/s13360-021-02180-7
16. A.S. Durmuslar, H. Dakhlaoui, M.E. Mora-Ramos, F. Ungan, Effects of external fields on the nonlinear optical properties of an n-type quadruple δ-doped GaAs quantum wells. Eur. Phys. J. Plus **137**, 730 (2022). https://doi.org/10.1140/epjp/s13360-022-02938-7
17. M.J. Karimi, H. Vafaei, Intenselaser field effects on the linear and nonlinear intersubband optical properties in astrained *InGaN/GaN* quantum well. Phys. B **452**, 131–135 (2014). https://doi.org/10.1016/j.physb.2014.07.001
18. F. Ungan, U. Yesilgul, S. Sakiroglu, E. Kasapoglu, H. Sari, I. Sökmen, Nonlinear optical absorption and refractive index in *GaInNAs/GaAs* double quantum wells under intense laser field and applied electric field. J. Lumin. **143**, 75–80 (2013). https://doi.org/10.1016/j.jlumin.2013.04.047
19. H. Dakhlaoui, J.A. Vinasco, C.A. Duque, External fields controlling the nonlinear optical properties of quantum cascade laser based on staircase-like quantum wells. Superlatt. Microstruct. **155**, 106885 (2021). https://doi.org/10.1016/j.spmi.2021.106885
20. A. Turkoglu, H. Dakhlaoui, M.E. Mora-Ramos, F. Ungan, Optical properties of a quantum well with Razavy confinement potential: role of applied external fields. Phys. E **134**, 114919 (2021). https://doi.org/10.1016/j.physe.2021.114919
21. H. Sari, F. Ungan, S. Sakiroglu, U. Yesilgul, I. Sokmen, The effects of intense laser field on optical responses of n-type delta doped GaAs quantum well under applied electric and magnetic fields. Optik **162**, 76–80 (2018). https://doi.org/10.1016/j.ijleo.2018.02.092
22. A. Tiutiunnyk, M.E. Mora-Ramos, A.L. Morales, C.M. Duque, R.L. Restrepo, F. Ungan, J.C. Martínez-Orozco, E. Kasapoglu, C.A. Duque, Electron Raman scattering in a double quantum well tuned by an external nonresonant intense laser field. Opt. Mater. **64**, 496–501 (2017). https://doi.org/10.1016/j.optmat.2017.01.001
23. M. Bati, The effects of the intense laser field on the resonant tunneling properties of the symmetric triple inverse parabolic barrier double well structure. Phys. B **594**, 412314 (2020). https://doi.org/10.1016/j.physb.2020.412314
24. S. Adachi, *GaAs and Related Materials: Bulk Semiconducting and Superlattice Properties* (World Scientific, Singapore, 1994)
25. J.-B. Xia, W.-J. Fan, Electronic structures of superlattices under in-plane magnetic field. Phys. Rev. B **40**, 8508 (1989). https://doi.org/10.1103/PhysRevB.40.8508
26. F. Ungan, Intensity-dependent nonlinear optical properties in a modulation-doped single quantum well. J. Lumin. **131**, 2237 (2011). https://doi.org/10.1016/j.jlumin.2011.06.003
27. R.L. Restrepo, E. Kasapoglu, S. Sakiroglu, F. Ungan, A.L. Morales, C.A. Duque, Second and third harmonic generation associated to infrared transitions in a Morse quantum well under applied electric and magnetic fields. Infrared Phys. Technol. **85**, 147 (2017). https://doi.org/10.1016/j.infrared.2017.06.005
28. H.S. Aydinoglu, S. Sakiroglu, H. Sari, F. Ungan, I. S¨okmen, Nonlinear optical properties of asymmetric double-graded quantum wells. Philos. Mag. A **98**, 2151 (2018). https://doi.org/10.1080/14786435.2018.1476785
29. J.C. Martinez-Orozco, K.A. Rodriguez-Magdaleno, J.R. Suarez-Lopez, C.A. Duque, R.L. Restrepo, Absorption coefficient and relative refractive index change for a double δ-doped GaAs MIGFET-like structure: electric and magnetic field effects. Superlatt. Microstruct. **92**, 166–173 (2016). https://doi.org/10.1016/j.spmi.2016.02.034

30. S. Baskoutas, C. Garoufalis, A.F. Terzis, Linear and nonlinear optical absorption coefficients in inverse parabolic quantum wells under static external electric field. Eur. Phys. J. B **84**, 241–247 (2011). https://doi.org/10.1140/epjb/e2011-20470-9
31. H. Dakhlaoui, Tunability of the optical absorption and refractive index changes in step-like and parabolic quantum wells under external electric field. Optik **168**, 416–423 (2018). https://doi.org/10.1016/j.ijleo.2018.04.109